Magnetoplasma excitations in electron rings

E. Zaremba
Department of Physics, Queen's University, Kingston, Ontario, Canada K7L 3N6
(Received 19 July 1995)

Magnetoplasma excitations in two-dimensional electron rings are studied using a hydrodynamic theory based on the Thomas–Fermi–Dirac–von Weizsäcker approximation to the electronic ground state. This system is found to support a rich spectrum of excitations including bulk and edge magnetoplasmons. Good agreement between theory and experiment is found with respect to the magnetic-field dispersion of the modes and their dependence on the ratio of the inner to outer ring diameters. [S0163-1829(96)51816-3]

In this paper we present a calculation of the magnetoplasma excitations in two-dimensional electron rings. These systems have recently been studied experimentally[1] and have been shown to exhibit excitations which have characteristics of both quantum dots[2] and antidot arrays.[3] We make use of a hydrodynamic approach which is based on the Thomas–Fermi–Dirac–von Weizsäcker (TFDW) approximation of the equilibrium electronic structure. The method was previously developed[4] in the context of three-dimensional (3D) parabolic wells, where it was shown to provide a realistic description of the magnetoplasma excitations in that geometry. Our purpose here is to show that the same method can also be used to account for the excitations in the ring geometry and to provide an interpretation of the various modes that have been observed experimentally. There have been a few previous calculations in this geometry: two are self-consistent field calculations with an idealized ring geometry[5] and another is a hydrodynamic calculation[6] in the so-called fully screened limit. Neither of these apply directly to the experimental situation of interest.

The experimental system studied previously[1] consisted of a two-dimensional electron gas with density $n_s = 2.3 \times 10^{11}$ cm^{-2}, which was patterned into an array of rings arranged on a square lattice. The rings were fabricated with an outer diameter of approximately 50 μm and an inner diameter of either 12 μm (wide rings) or 30 μm (narrow rings). As we shall show, the important geometrical parameter determining the character of the modes is the aspect ratio of the inner to outer diameters.

Because of the large physical size of the experimental rings and their proximity to a neutralizing positive background provided by ionized donor impurities, it is reasonable to consider a model in which the electrons and positive background are confined to a plane. The positive background itself has the geometry of a ring with the desired aspect ratio and is chosen to have a uniform density equal to that of the electron gas in the experiments. With this definition of the external electrostatic potential confining the electrons, the equilibrium properties are determined from the TFDW energy functional

$$E[n] = \int d\mathbf{r}\left[C_1 n^2 + C_2 \frac{|\nabla n(\mathbf{r})|^2}{n(\mathbf{r})} - C_3 n^{3/2} \right] + \frac{1}{2}\int d\mathbf{r} \int d\mathbf{r}' \frac{n(\mathbf{r}) n(\mathbf{r}')}{|\mathbf{r}-\mathbf{r}'|} + \int d\mathbf{r}\, v_{\rm ext}(\mathbf{r}) n(\mathbf{r}), \quad (1)$$

where $n(\mathbf{r})$ is the two-dimensional electron density distribution. The first term is the Thomas-Fermi kinetic energy, the second term is the von Weizsäcker correction to the kinetic energy, and the third term is the Dirac local exchange energy. The Thomas-Fermi and exchange[7] energies are written in a form suitable for a two-dimensional situation with coefficients $C_1 = \pi/2$ and $C_3 = \frac{4}{3}\sqrt{2/\pi}$, respectively (we use atomic units $e^2/\epsilon = m^* = \hbar = 1$ throughout). In the von Weizsäcker coefficient $C_2 = \lambda_w/8$, the λ_w parameter is chosen to have the value 0.25, which was found in other applications to provide the best agreement between the TFDW and full density-functional calculations.[8] The last two terms in Eq. (1) are the Hartree and external energies.

The equilibrium density is found by minimizing $E[n]$ subject to the constraint of a fixed number of electrons N. By defining the von Weizsäcker ''wave function'' $\psi(\mathbf{r}) = \sqrt{n(\mathbf{r})}$, the equilibrium condition is equivalent to the solution of the Schrödinger-like equation,

$$-\frac{\lambda_w}{2}\nabla^2 \psi(\mathbf{r}) + v_{\rm eff}(\mathbf{r})\psi(\mathbf{r}) = \mu \psi(\mathbf{r}), \quad (2)$$

where μ is the chemical potential and

$$v_{\rm eff}(\mathbf{r}) = 2C_1 \psi^2(\mathbf{r}) - \tfrac{3}{2} C_3 \psi(\mathbf{r}) + \phi(\mathbf{r}) + v_{\rm ext}(\mathbf{r}). \quad (3)$$

Here $\phi(\mathbf{r}) = \int d\mathbf{r}' n(\mathbf{r}')/|\mathbf{r}-\mathbf{r}'|$ is the Coulomb potential. The self-consistent solution of Eqs. (2) and (3) with the normalization $\int d\mathbf{r}\psi^2(\mathbf{r}) = N$ yields the equilibrium wave function $\psi_0(\mathbf{r})$ and density $n_0(\mathbf{r})$.

The dynamics of the electrons in the presence of a perpendicular magnetic field $\mathbf{B}$ is described using the linearized hydrodynamic equations,[4]

$$\frac{\partial \delta n}{\partial t} + \nabla \cdot (n_0 \mathbf{v}) = 0, \quad (4)$$

$$\frac{\partial \mathbf{v}}{\partial t} = \delta \mathbf{F} - \frac{e}{c}\mathbf{v} \times \mathbf{B}, \quad (5)$$

where the density fluctuation is $\delta n = 2\psi_0 \delta\psi$ and the internal force fluctuation is

$$\delta \mathbf{F} = -\nabla\left[\delta v_{\rm eff} + \frac{1}{\psi_0}\hat{h}\,\delta\psi \right] \equiv -\nabla f. \quad (6)$$

The term involving the ground-state Hamiltonian

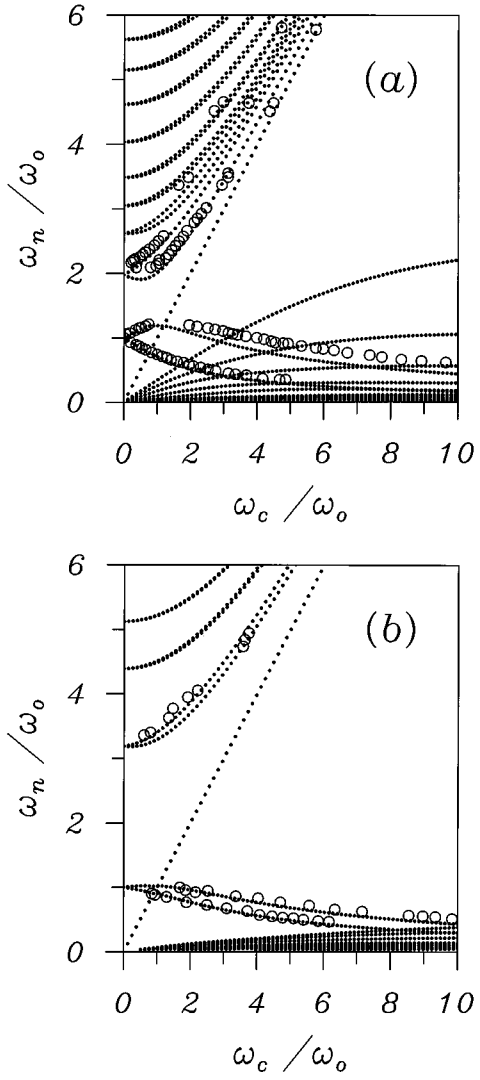

FIG. 1. Mode frequencies as a function of magnetic field; (a) is for the wide ring ($d_1/d_2=0.24$) and (b) is for the narrow ring ($d_1/d_2=0.58$). The open circles are the experimental results (Ref. 1), scaled by the zero-field frequency, as explained in the text. The upper and lower branches starting from $\omega_n/\omega_0=1$ correspond to ω_{0+} and ω_{0-}, respectively; the next two branches with increasing frequency correspond to ω_{1+} and ω_{1-}.

$$\hat{h}=-\frac{\lambda_w}{2}\nabla^2+(v_{\rm eff}^0-\mu) \tag{7}$$

arises from the von Weizsäcker term in the energy functional.

The solution of Eqs. (4)–(6) is achieved by expanding the fluctuating variables ($\propto e^{-i\omega t}$) in a complete set of functions defined by $\hat{h}\varphi_i=\mu_i\varphi_i$. Specifically, we have $\delta\psi=\Sigma_i c_i\varphi_i$ and $\psi_0 f=\Sigma_i f_i\varphi_i$ with the expansion coefficients related by $f_i=\Sigma_j\tilde{M}_{ij}c_j$. The matrix $\tilde{M}_{ij}$ follows from the definition of f in Eq. (6) and is given explicitly in our earlier work.[4] Substitution of these expansions in Eqs. (4) and (5) with the elimination of the velocity field $\mathbf{v}$ leads to the generalized eigenvalue problem

$$\omega(\omega^2-\omega_c^2)\sum_j \tilde{M}_{ij}^{-1}f_j=\frac{\mu_i}{\lambda_w}\omega f_i+i\omega_c\sum_j A_{ij}f_j, \tag{8}$$

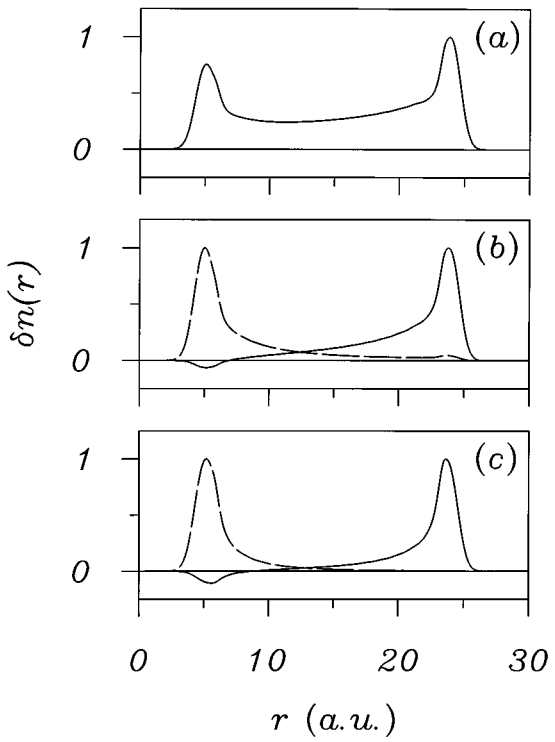

FIG. 2. Mode densities as a function of the radial distance for the ω_{0-} mode (solid line) and the ω_{0+} mode (dashed line). Panels (a), (b), and (c) correspond to magnetic fields of $B=0$, 2, and 4 T, respectively; at $B=0$ T both modes have the same density.

with

$$A_{ij}=\int d^2r\,\ln\psi_0\left(\frac{\partial\varphi_i^*}{\partial y}\frac{\partial\varphi_j}{\partial x}-\frac{\partial\varphi_i^*}{\partial x}\frac{\partial\varphi_j}{\partial y}\right). \tag{9}$$

Here, $\omega_c=eB/m^*c$ is the cyclotron frequency. The solutions of Eq. (8) define the mode frequencies and corresponding mode eigenvectors.

For the ring geometry with circular symmetry, the basis functions have the form $\varphi_{nm}(\mathbf{r})=u_{nm}(r)e^{im\theta}$ where m is an azimuthal quantum number and n is a radial index. In this case, $\tilde{M}_{nm,n'm'}$ and $A_{nm,n'm'}$ are diagonal in the m index and Eq. (8) reduces to an independent set of equations for each m value. The dipolar modes of interest have $m=\pm1$.

In Fig. 1 we show the dipole mode dispersion as calculated for rings with $N=400$. Although the absolute values of the mode frequencies depend on the electron number N, the frequencies, scaled by the lowest nonzero $B=0$ eigenfrequency ω_0, are found to be approximately N independent as a function of the scaled cyclotron frequency. When the theoretical and experimental results are plotted in this way, it can be seen that there is a very good correspondence between the observed mode frequencies and a subset of the theoretical modes for both aspect ratios studied experimentally.

Since Eq. (8) is a cubic equation in ω, the eigenfrequencies appear in threes with one pair being degenerate at $B=0$ and the third having a zero limiting frequency as $B\to0$. The latter modes are analogous to those found in the dot geometry[9] and will be discussed in more detail shortly. The remaining modes which have a finite limiting value at $B=0$ are of more experimental interest since only these have an

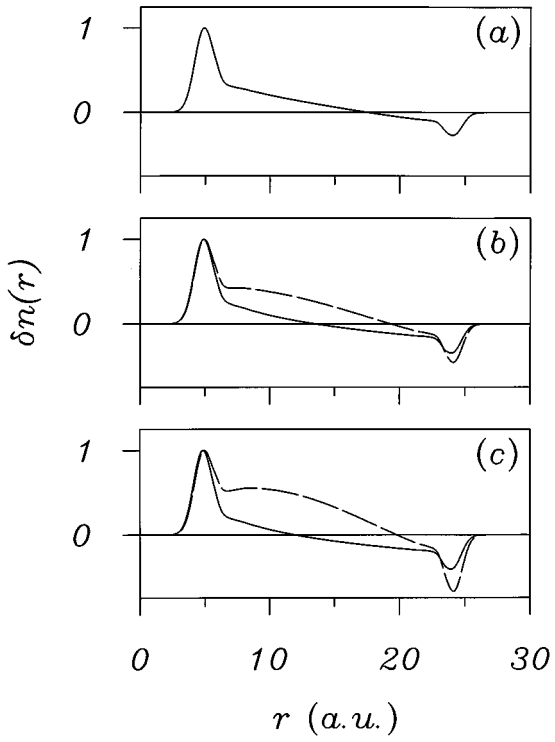

FIG. 3. As in Fig. 2, but for the ω_{1+} mode (solid line) and the ω_{1-} mode (dashed line).

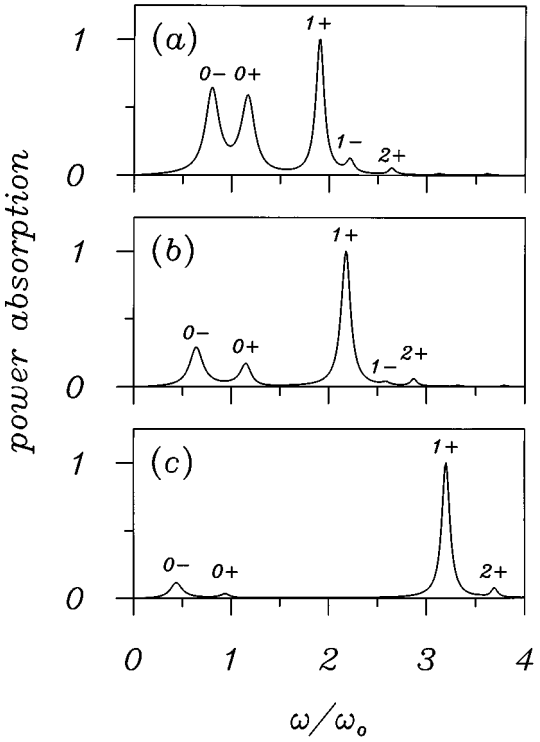

FIG. 4. The calculated power absorption for the wide ring as a function of the excitation frequency at magnetic fields of (a) 1 T, (b) 2 T, and (c) 4 T ($\omega_c/\omega_0=0.68$, 1.36, and 2.72, respectively). The various peaks are identified by the mode index.

observable oscillator strength when excited by a uniform external electric field. These modes, denoted by $\omega_{n\pm}$, are the dipolar magnetoplasma excitations. The index $n=0,1,...$ represents the number of radial nodes in the mode densities, while the ''+'' and ''−'' designation distinguishes the counterclockwise and clockwise sense of angular rotation, respectively. The pair of frequencies, $\omega_{0\pm}$, decreasing with increasing B for large B correspond to edge magnetoplasmons (EMP). The remaining modes with $n\neq 0$ asymptotically approach the cyclotron frequency and represent bulk magnetoplasmons.

The mode density of $\omega_{0\pm}$ at $B=0$ is shown in Fig. 2(a). The density distribution is almost symmetric with respect to the midpoint of the ring and is the analogue of the 1D plasmon in a straight 1D wire with a wavelength equal to the mean circumference of the ring $[\lambda\simeq\frac{1}{2}\pi(d_1+d_2)]$. The slight asymmetry is a consequence of the wire being bent into a ring. In Figs. 2(b) and 2(c) we show the $\omega_{0\pm}$ mode densities at higher fields. In contrast to the parabolic center-of-mass modes which have the *same* density distribution for both modes at all magnetic fields,[9,10] the ring $\omega_{0\pm}$ modes are the same only at $B=0$ and then display a very strong variation with increasing field. At higher fields they evolve into EMP's localized at the inner (ω_{0+}) and outer (ω_{0-}) edges of the ring. The frequency splitting can be understood simply in view of the wave-vector dispersion $[\omega(k)\propto k\ \ln(1/|ka|)]$ of the EMP in the semi-infinite plane[11] and the fact that the ring EMP's have different effective wave numbers, $k\simeq 2/d_1$ for ω_{0+} and $k\simeq 2/d_2$ for ω_{0-}. This also explains why the modes approach each other with increasing aspect ratio, as is evident on going from Figs. 1(a) to 1(b). In the linear strip geometry $(d_1/d_2\rightarrow 1)$, the two EMP's propagating in opposite directions on the two sides of the strip are degenerate for the same wave vector.

In Figs. 3(a)–3(c) we show the mode densities for the $\omega_{1\pm}$ modes. These modes have a single radial node and are therefore dipolar in character *across* the width of the ring. With increasing magnetic field the ω_{1+} mode density tends to concentrate on the outer edge of the ring, whereas the ω_{1-} mode has the opposite tendency. These modes are the first in a series of bulk magnetoplasmons with an increasing number of radial nodes.

Of all the modes displayed in Fig. 1, only a few are strongly excited by a uniform electric field. To illustrate this we show in Fig. 4 the power absorption as a function of the excitation frequency at magnetic fields of 1, 2, and 4 T $(\omega_c/\omega_0=0.68$, 1.36, and 2.72). These results are obtained by adding an additional driving term to the right-hand side of Eq. (5), together with a phenomenological damping term which gives the resonances a finite width. In an earlier study of electron dots,[10] we found that a damping rate inversely proportional to frequency provided the most realistic description of the observed widths. This same assumption is used here, although it should be stressed that whether or not the damping has this form has no influence on the relative strength of the resonances. At zero magnetic field, the $\omega_{0\pm}$ modes are degenerate and carry the bulk of the oscillator strength, although the strength of the degenerate $\omega_{1\pm}$ modes is also appreciable. With increasing magnetic field, the ω_{0+} mode becomes weaker relative to the ω_{0-} mode, and both of these modes lose intensity with respect to the $\omega_{1\pm}$ modes. Although the two ω_1 modes start off with equal intensity, the ω_{1-} mode rapidly loses strength relative to the ω_{1+} mode so that by $B=4$ T, the ω_{1-} mode is unobservable. This is precisely the behavior seen experimentally in the

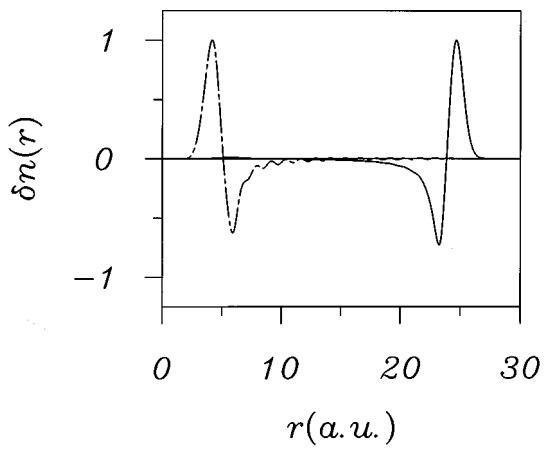

FIG. 5. Examples of the dipole edge magnetoplasmons for the wide ring at $B=4$ T. The inner (dashed) EMP rotates counterclockwise and the outer (solid) EMP clockwise. The small ripples are an artifact of the basis set truncation.

wide ring for which the ω_{1-} branch terminates at $\omega_c/\omega_0 \simeq 1.5$. Of the remaining calculated resonances, the ω_{2+} mode is the strongest and presumably corresponds to one of the higher frequency experimental modes displayed in Fig. 1(a).

Finally, we turn to the series of modes which start at zero frequency and disperse linearly with B at small fields. As Fig. 4 shows, none of these modes has observable dipole oscillator strengths and no evidence of them was seen experimentally. They are analogous to the modes first found in parabolically confined quantum dots[9] and more recently at the edge of a two-dimensional[12,13] and three-dimensional electron gas.[4] In the 2D geometry, these modes have a linear wave-vector dispersion and are therefore referred to as ''acoustic'' excitations. As emphasized by Aleiner and Glazman,[12] their existence depends crucially on the fact that the electron density varies smoothly at the edge of the bounded electronic system. In Fig. 5 we illustrate the typical character of some of these modes at a magnetic field of 4 T. In comparison to Fig. 2(c), it can be seen that the mode densities have a node in the surface region and are therefore dipolar in character. In this sense, these modes can be classified as multipolar EMP's in contrast to the monopolar $\omega_{0\pm}$ modes.

In summary, we have shown that the TFDW hydrodynamic theory provides a good description of the magnetoplasma excitations in electron rings. In particular, the theory accounts for the observed dependence of the magnetic-field dispersion on the aspect ratio. Our calculation of the power absorption confirms the original classification[1] of the modes observed experimentally, and the explicit calculation of mode densities provides a more complete understanding of the physical nature of these excitations.

This work was supported by a grant from the Natural Sciences and Engineering Research Council of Canada. I would like to thank Z. L. Ye for help with the numerical computations.

[1] C. Dahl, J. P. Kotthaus, H. Nickel, and W. Schlapp, Phys. Rev. B **48**, 15 480 (1993).
[2] T. Demel, D. Heitmann, P. Grambow, and K. Ploog, Phys. Rev. Lett. **64**, 788 (1990).
[3] K. Kern, D. Heitmann, P. Grambow, Y. H. Zhang, and K. Ploog, Phys. Rev. Lett. **66**, 1618 (1991).
[4] E. Zaremba and H. C. Tso, Phys. Rev. B **49**, 8147 (1994).
[5] D. Huang and G. Gumbs, Phys. Rev. B **46**, 4147 (1992); D. Huang, Y. Zhu, Z. Liu, and S. Zhou, *ibid*. **39**, 7713 (1989).
[6] C. R. Proetto, Phys. Rev. B **46**, 16 174 (1992).
[7] A. V. Chaplik, Zh. Eksp. Teor. Fiz. **60**, 1845 (1971) [Sov. Phys. JETP **33**, 947 (1971)]; F. Stern, Phys. Rev. Lett. **30**, 278 (1973).
[8] A. Chizmeshya and E. Zaremba, Phys. Rev. B **37**, 2805 (1988).
[9] S. S. Nazin and V. B. Shikin, Zh. Eksp. Teor. Fiz. **94**, 133 (1988) [Sov. Phys. JETP **67**, 288 (1988)]; Fiz. Nizk. Temp. **15**, 227 (1989) [Sov. J. Low Temp. Phys. **15**, 127 (1989)].
[10] Z. L. Ye and E. Zaremba, Phys. Rev. B **50**, 17 217 (1994).
[11] V. A. Volkov and S. A. Mikhailov, Zh. Eksp. Teor. Fiz. **94**, 217 (1988) [Sov. Phys. JETP **67**, 1639 (1988)].
[12] I. L. Aleiner and L. I. Glazman, Phys. Rev. Lett. **72**, 2935 (1994).
[13] I. L. Aleiner, D. Yue, and L. I. Glazman, Phys. Rev. B **51**, 13 467 (1995).